Published in final edited form as:

*Cell Rep*. 2017 August 08; 20(6): 1262–1268. doi:10.1016/j.celrep.2017.07.042.

# Extended interneuronal network of the dentate gyrus

**Gergely G. Szabo**[1], **Xi Du**[2], **Mikko Oijala**[1], **Csaba Varga**[1,3], **Jack M. Parent**[2,4], and **Ivan Soltesz**[1]

[1]Department of Neurosurgery, Stanford University, Stanford, CA 94305, USA

[2]Department of Neurology, University of Michigan, Ann Arbor, MI 48109, USA

[4]VA Ann Arbor Healthcare System, MI 48109, USA

## SUMMARY

Local interneurons control principal cells within individual brain areas, but anecdotal observations indicate that interneuronal axons sometimes extend beyond strict anatomical boundaries. Here we use the case of the dentate gyrus (DG) to show that boundary-crossing interneurons with cell bodies in the CA3 and CA1 constitute a numerically significant and diverse population that relays patterns of activity generated within the CA regions back to granule cells. These results reveal the existence of a sophisticated retrograde GABAergic circuit that fundamentally extends the canonical interneuronal network.

## eTOC blurb

Szabo et al. describe an extended interneuronal network in the hippocampal circuitry that supplies the dentate gyrus with GABAergic inhibition and includes external interneurons. Such boundary-crossing cells channel sharp wave ripple-related activity patterns from the downstream CA regions back to the dentate gyrus.

Corresponding author (lead contact): Gergely G. Szabo, PhD, Department of Neurosurgery, Stanford University Stanford CA 94305, USA, szergely@stanford.edu.

[3]Present address: Szentágothai Research Center, Department of Physiology, Medical School, University of Pécs, NAP-B Entorhinal Microcircuits Research Group, Pécs, 7624 Hungary

**AUTHOR CONTRIBUTIONS**

G.G.S. and I.S. conceived the project. G.G.S. and X.D. performed and analyzed the juxtacellular and presynaptic tracing experiments, respectively. M.O. wrote the analysis software and C.V. contributed to the design and setting up of the juxtacellular experiments. I.S. and J.P. supervised the study, G.G.S. and I.S. wrote the paper with assistance from all authors.

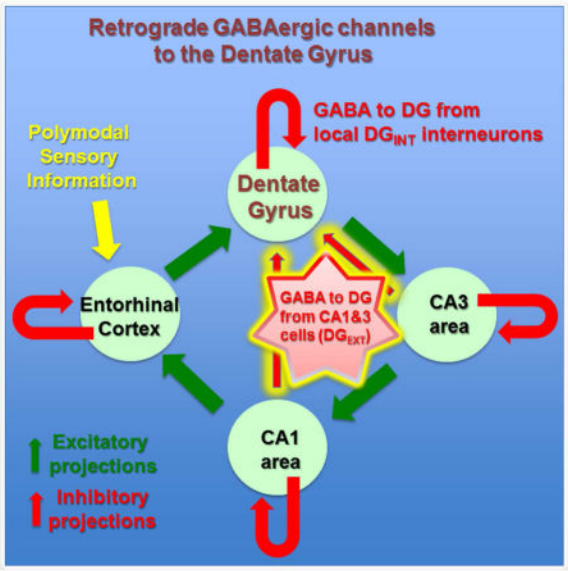


**Keywords**

GABA; inhibition; hippocampus; network

## INTRODUCTION

Two main types of GABAergic cells are currently recognized to exert inhibitory control over principal cell populations in cortical circuits. The first group is comprised of the classical interneuronal subtypes, which in the hippocampus includes interneurons such as the axo-axonic (chandelier), basket and oriens-lacunosum moleculare cells. These interneurons, sometimes referred to as local circuit interneurons, are specialized to release GABA onto the different postsynaptic domains of the nearby excitatory principal cells that form the output channels to other brain regions, and most subtypes can also innervate, albeit less frequently, other interneurons located within the same anatomically defined brain area. The second major GABAergic cell group is formed by the long-distance projecting cells, which are increasingly being recognized as key players in gating the flow of information between distant brain regions, often by selectively synapsing on interneurons in the target area (Basu et al., 2016; Melzer et al., 2012). Within the hippocampal formation, each of the anatomically defined regions such as the dentate gyrus (DG), CA3 and CA1 area has a certain number of “classical” interneurons (e.g., 27,240 in the rat CA1 (Bezaire and Soltesz, 2013)) that regulate local principal cell excitability, whereas long-distance projecting GABA cells from the medial septum and entorhinal cortices exert powerful behavioral state-dependent control over local hippocampal circuits through various disinhibitory gating mechanisms (Basu et al., 2016; Melzer et al., 2012). Interestingly, several studies contain anecdotal observations indicating that axons of hippocampal interneurons sometimes cross the classical anatomically defined areal boundaries (Hájos and Mody, 1997; Katona et al., 2016; Lasztóczi et al., 2011; Sik et al., 1994; Szabadics and Soltesz, 2009; Szabó et al., 2014; Ceranik et al., 1997; Armstrong et al., 2011), indicating the possible existence of a

third major GABAergic cell class that extends its influence from the local networks to the immediately adjacent circuits. However, the existence, abundance, cellular composition and functional properties of such an extended, meso-scale (i.e., between local circuit and long-distance) interneuronal system are not well understood. We focused on the DG to gain insights into the hypothesized extended interneuronal system, since the local (i.e., within-DG) interneuronal subtypes supplying inhibition to the DG granule cells (GCs) are relatively well described and are known to play key roles in the regulation of informational flow from the entorhinal cortex to the downstream CA regions (Hosp et al., 2014).

## RESULTS

### Extrinsic interneurons located in CA3 and CA1 form a significant portion of GABAergic inputs to dentate granule cells (GCs)

First, we sought to estimate the relative abundance of the classical, intrinsic ($DG_{INT}$) versus the extrinsic ($DG_{EXT}$; i.e., cell bodies outside the DG with axonal projections to the DG) interneurons that innervate GCs. We used a dual retroviral and rabies strategy (see Methods) to label the presynaptic partners of mature GCs. The retrograde trans-synaptic labeling revealed non-principal presynaptic cells located not only within the DG but also in the CA3 and CA1 areas. Subsequent immunocytochemical analysis of two key markers for major interneuron classes (parvalbumin, PV; and somatostatin, SOM) showed that the relative numerical abundance of $DG_{EXT}$ was about 15%–20% of the total presynaptic PV/SOM population (Fig. 1; presynaptically labeled PV cells, $DG_{INT}$: 79.12±11.51%; $DG_{EXT}$ in CA3: 12.64±5.5%; $DG_{EXT}$ in CA1: 8.24±12.21%; presynaptically labeled SOM cells, $DG_{INT}$: 83.52±9.92%; $DG_{EXT}$ in CA3: 11.30±7.44%; $DG_{EXT}$ in CA1: 5.18±7.34%; $N$=6 animals). Therefore, extrinsic GABA cells in the CA1&3 with retrograde projections to the DG include at least two major non-principal cell classes (PV and SOM), and these cells collectively contribute to the extended interneuronal network of the DG in a numerically significant manner. In addition, these data indicate that the axons of the $DG_{EXT}$ PV and SOM interneurons are likely to form close contacts with GCs.

### Both perisomatic- and dendrite-targeting $DG_{INT}$ interneurons are modulated by sharp wave-ripples (SWRs) and dentate spikes

Next, we examined the *in vivo* functional properties of the extended interneuronal network innervating the DG using juxtacellular recordings from individual cells in awake head-fixed mice. The juxtacellular technique is a low throughput but non-invasive technique (i.e., it does not disturb the intracellular milieu of the recorded cell) that allows the rigorous post-hoc identification of the recorded neurons (Varga et al., 2012, 2014). All cells in the database of this paper had their axonal and dendritic arborizations visualized for morphology-based cell identification, and 19 of the 22 cells were also immunocytochemically identified (for cell reconstructions of various $DG_{INT}$ and $DG_{EXT}$ interneuron types, see Figs. S1 and S2, respectively). We focused on the discharges of the recorded cells during sharp wave ripples (SWRs), because these cognitively important (Girardeau et al., 2009), fast electrographic network events are known to be generated in the CA circuits downstream from the DG (Oliva et al., 2016), offering a unique opportunity to gain insights into the possibility of retrograde channeling of the CA1&3 activity back to the DG. First, we compared the SWR-

related activity patterns of the $DG_{INT}$ and $DG_{EXT}$ interneurons, with the SWRs recorded from the CA1 pyramidal cell layer with a separate local field potential (LFP) electrode. Previous observations using extracellular recordings demonstrated that spiking activity of unidentified cells in the hilar region can be modulated by SWRs (Penttonen et al., 1997). In agreement with these earlier reports, $DG_{INT}$ PV positive, fast spiking basket cells (FSBCs; n=3) innervating the perisomatic regions of GCs significantly increased their firing during SWRs (outside SWR: 16.6±4.7Hz, inside: 36.9±8.7Hz, n=3; P=0.041; Fig 2A, C, E). Dendrite-targeting cells among the $DG_{INT}$ cell group belonged to the SOM class (n=3) (Fig 2B,D; in addition, we also successfully recorded and recovered the first *in vivo* examples of nitrogen-monoxide synthase 1 expressing (NOS; n=1) and cannabinoid type I receptor expressing (CB1; n=2) $DG_{INT}$ cells as well (Fig. S1)). The dendrite-targeting SOM $DG_{INT}$ cells exhibited significant increases in activity during SWRs (outside SWR: 4.7±3.2Hz, inside: 9.6±4.6Hz, n=3; P=0.045; Fig 2E; similarly to the NOS but not the CB1 $DG_{INT}$ neurons, see Fig 2 legend). Therefore, at least two (PV and SOM, i.e., including both perisomatic- and dendrite-targeting cells) out of the four major $DG_{INT}$ interneuronal groups that are known to innervate DG GCs (PV, SOM, NOS, CB1 cells) receive information about SWR events generated in the downstream CA areas and exhibit marked SWR-related changes in action potential discharges. Interestingly, similar increases in perisomatic- and dendrite-targeting $DG_{INT}$ interneuron discharges could also be observed during a different type of fast network event, the dentate spikes (perisomatic-targeting cells: outside dentate spikes: 10.2±3.4Hz, inside dentate spikes: 108.1±17.3Hz, n=3; dendrite-targeting cells: outside: 4.4±1.1Hz, inside: 26.4±7.7Hz, n=5, Fig 2F–H). Since dentate spikes originate in the DG in response to a sudden surge in incoming excitatory afferent activity from the entorhinal cortex (Bragin et al., 1995; Penttonen et al., 1997), these data indicate that both upstream and downstream networks can impose fast temporal modulation on $DG_{INT}$ discharges.

## Diversity of perisomatic- and dendrite-targeting $DG_{EXT}$ interneurons and their modulation by SWRs

Next, we obtained juxtacellular recordings from $DG_{EXT}$ interneurons. The somata of these cells (n=10) were located in the CA1 or CA3 regions, and had axonal projections of varying densities in the DG. Similar to the $DG_{INT}$ interneurons, immunocytochemical analysis showed that the $DG_{EXT}$ cells comprised several major interneuronal classes and consisted of both perisomatic-targeting and dendrite-targeting cells (Fig 3A–D; Fig S2). Therefore, an extended interneuronal system exists that supplies GABAergic inputs to the DG, and the diversity of the $DG_{EXT}$ retrograde interneuronal network rivals that of the $DG_{INT}$ interneurons (Fig 3E). Interestingly, the synaptic targeting preferences of the $DG_{EXT}$ interneurons was broadly preserved across hippocampal regions, as indicated by the fact that cells that innervated dendritic layers in the CA1 or CA3 regions (i.e., strata radiatum and lacunosum-moleculare) where their cell bodies resided also targeted dendritic layer in the dentate gyrus (stratum moleculare), and a similar preservation of targeting rules was also observed for the perisomatic-targeting cells (Fig. S2F).

Importantly, all $DG_{EXT}$ interneurons showed significant modulation in their firing during SWRs (Fig 3F), with SOM $DG_{EXT}$ (n=3) and NOS $DG_{EXT}$ (n=4) cells increasing, whereas

the PV $DG_{EXT}$ axo-axonic (chandelier) cells (n=2) and the CB1 $DG_{EXT}$ cell (n=1) decreasing their discharges. As a group, $DG_{EXT}$ had significantly higher spiking rate inside than outside SWRs (inside: 31±14.2Hz; outside: 4.6±0.9Hz, n=10, P=0.047). Therefore, these data indicate that the DG receives SWR-modulated patterns of GABAergic release through these $DG_{EXT}$ neurons as well. Comparison of the SWR-related changes in the firing of the $DG_{EXT}$ and $DG_{INT}$ revealed that the extrinsic cell population showed significantly larger alterations in spiking rates compared to the intrinsic cells, consistent with most of their dendrites located within the CA networks that generate SWR activity (Fig 3G).

### Temporal dynamics of SWR-dependent modulation of interneuronal firing

Next, we examined the question of the temporal distribution of the ensemble GABAergic inputs that the DG receives from the extended (i.e., the $DG_{INT}$ and $DG_{EXT}$) interneuronal network. When the $DG_{INT}$ and $DG_{EXT}$ cells were examined as a unified population, the FSBCs and SOM cells (Fig 4A, D) increased their firing most prominently during the SWRs, whereas the NOS cells (Fig 4B, D) reached their peak increase in action potential discharges around 100ms after the middle of the SWRs. In contrast, a third group of cells (Fig 4C, D) displayed a biphasic modulation where the initial marked decrease in their firing during the SWRs was followed by a prominent but delayed rebound (Fig 4D, inset). Interestingly, all of these three groups contained both intrinsic and extrinsic cells (raster plots for the extrinsic cells are shown in Fig 4A–C; for their intrinsic counterparts, and additional examples of $DG_{EXT}$ at two time-scales, see Fig S4). Therefore, the extended interneuronal network as a whole provides a temporally distributed pattern of SWR-modulated inhibition to the DG neuronal network, with cell type-specific preferences in the SWR-related timing of peak discharges.

A fourth, distinct pattern emerged in the case of the $DG_{EXT}$ axo-axonic cells (n=2) whose cell bodies were located in the CA3c, with their axons innervating both the CA3 pyramidal cell and the DG GC layers (Fig 3A). Uniquely among all hippocampal interneurons reported here or in the literature (Varga et al., 2014; Viney et al., 2013), these cells bridging the CA3c and DG regions decreased their firing not only during the SWRs but also several hundreds of milliseconds before these events (Fig 4E; note that the cell in Fig 4E decreased its discharges > 1.5 sec before SWRs, even when only solitary SWRs that occurred without other SWRs within a 5 sec window were considered; Fig S3 I–J). These observations suggest that changes in GABA-release in the DG can take place far in advance of the onset of SWRs in the CA1, which may contribute to the observed changes in GC resting membrane potential prior to SWR onset (Hulse et al., 2017). Additional analysis showed that the cessation in firing during the SWRs observed in n=5 cells (2 $DG_{EXT}$ axo-axonic, 1 $DG_{EXT}$ CB1 and 2 hilar $DG_{INT}$) was most likely due to active inhibition and not a pause in incoming excitation (Fig. 4F–H), indicating that both select $DG_{EXT}$ and $DG_{INT}$ GABAergic cell populations can be subject to powerful inhibition during SWRs (Varga et al., 2014; Viney et al., 2013).

## DISCUSSION

Our results indicate that in addition to classical local interneurons and dedicated long-distance projecting GABA cells, there is also a third, numerically significant, meso-scale,

extended interneuronal network whose cellular diversity is comparable to the major interneuronal classes that are known to innervate principal cells in hippocampal networks. These data provide a conceptual framework for the previous anecdotal observations (Hájos and Mody, 1997; Katona et al., 2016; Lasztóczi et al., 2011; Sik et al., 1994; Szabadics and Soltesz, 2009; Szabó et al., 2014; Ceranik et al., 1997; Armstrong et al., 2011) of individual interneurons that possessed axon branches that extended out into neighboring regions from the anatomically defined area where the parent cell bodies were located. Remarkably, the extended interneuronal network as a whole seems to be able to provide both spatially (perisomatic and dendritic) and temporally (Fig 4D) distributed inhibition, likely contributing to the characteristically sparse firing of GCs. The axons of the $DG_{EXT}$ interneurons showed similar preferential innervation of the dendritic or somatic layers in the CA areas (where their cell bodies were located) and the DG. Therefore, the synaptic targeting rules characteristic of interneurons belonging to distinct classes appear to be broadly preserved across neighboring brain regions.

These results indicating that a large part of GABAergic inputs to principal cells may not originate from local interneurons present in a given circuit have important implications for recent efforts to create data-driven, full-scale biophysical models of individual hippocampal areas (Bezaire and Soltesz, 2013). For example, in the case of the CA1 network, it has been reported that about 39% of GABAergic synaptic contacts on pyramidal cells could not be assigned to any of the known CA1 interneuron classes (Bezaire and Soltesz, 2013), a seemingly puzzling observation that may now be readily explainable by the sizable contribution of boundary-crossing interneurons from adjacent areas. Finally, the present results also reveal retrograde channeling of SWR-related activity from the downstream CA areas back to the DG, providing a potential regulatory mechanism associated with the bidirectional DG-CA3 interplay hypothesized to play key roles in sharp-wave-associated episodic memory sequencing and replay (Lisman et al., 2005).

## EXPERIMENTAL PROCEDURES

### Animals

All animal procedures were performed in accordance with the Institutional Animal Care and Animal Use Committee (IACUC) of the University of California, Irvine and the University of Michigan, and with the Administrative Panel on Laboratory Animal Care (APLAC) at Stanford University. Juxtacellular recordings were performed in adult (4 to 14 month-old) male C57BL/6 mice (Jackson laboratories). Trans-synaptic labeling experiments were carried out in male Sprague-Dawley rats purchased from Charles River. For additional details, see Supplemental Information.

### Viral production and intrahippocampal injections

Retroviral construct (Syn-GTR) was generated using a vesicular stomatitis virus G-protein (VSV-G) pseudotyped Murine Moloney Leukemia virus-based vector containing a human Synapsin1 promoter driving green fluorescent protein (GFP), the avian sarcoma leukosis virus receptor TVA and RbV glycoprotein (Rgp). Titers ranged from $2–5 \times 10^8$ cfu/mL. Avian envelope glycoprotein subgroup A (EnvA)-pseudotyped RbV (RbV-mCh) was

produced as described previously (Wickersham et al., 2010) with titers of 1–8 × $10^8$ cfu/mL. We injected Syn-GTR bilaterally into the dorsal dentate gyrus at postnatal day (P) 7 as previously described (Althaus et al., 2016; Kron et al., 2010) to birthdate neonatally-born dentate granule cells and render them RbV-competent. For additional details, see Supplemental Information.

### Juxtacellular recordings and related surgical procedures

Anesthesia and surgical procedures were performed as described previously (Varga et al., 2012, 2014). Briefly, stainless steel head bars were affixed to the skull during deep isoflurane anesthesia. On the day of the experiment a small (1mm) craniotomy was made over the right or left hippocampus (−2 mm antero-posterior and 2 mm lateral) under isoflurane anesthesia. Mice were then placed onto an 8-inch spherical treadmill and recording began once the animals had recovered. For additional details and for cell labelling procedure, see Supplemental Information.

### Immunohistochemistry on trans-synaptically labeled samples

On day 7 after RbV-mCh injection, animals were deeply anesthetized with pentobarbital and transcardially perfused with 0.9% saline and 4% paraformaldehyde (PFA). Brains were removed and post-fixed overnight in 4% PFA and cryoprotected with 30% sucrose. Frozen coronal sections (40 μm thickness) were cut in the coronal plane using a sliding microtome for subsequent immunohistochemical processing. For more details, see Supplementary Information.

### Analysis of electrophysiological data

Recordings were split into parts corresponding to “run” and “rest” episodes based on the video recordings. Only “rest” periods were used for this study, and their duration ranged between 350 and 771 sec. Data analysis was performed utilizing custom Matlab scripts as described previously (Varga et al., 2012, 2014) with additional features and modifications as described in the Supplemental Information.

### Statistics

Statistical comparisons were made using Origin Pro 9.0 (Origin Corp., Northampton, MA). For all datasets, normality was tested using Kolmogorov-Smirnov test and further parametric or nonparametric statistical approaches were selected accordingly. For dependent samples paired t-test was used. Multiple groups of data were compared using the nonparametric Kruskal-Wallis ANOVA test, followed by comparison of sample pairs using the Mann-Whitney *U*-test. $P<0.05$ was considered a significant difference. With the exceptions of Fig 3G and the inset on Fig 4D, data are presented as mean and the individual values or mean. In the main text, data is expressed as mean ± standard deviation unless stated otherwise.

## Supplementary Material

Refer to Web version on PubMed Central for supplementary material.

## Acknowledgments

We thank the Stanford Neuroscience Microscopy Service (supported by NIH NS069375) for technical support. We thank Rose Zhu, Theresa Nguyen and Sylwia Felong for technical assistance. We are also grateful to Artur Luczak for useful comments on an early version of the manuscript. This work was supported by the NIH (NS35915 and NS090583 to I.S.; NS058585 to J.M.P) and the George E. Hewitt Foundation for Medical Research (to G.G.S.).

## References

Althaus AL, Zhang H, Parent JM. Axonal plasticity of age-defined dentate granule cells in a rat model of mesial temporal lobe epilepsy. Neurobiol Dis. 2016; 86:187–196. [PubMed: 26644085]

Armstrong C, Szabadics J, Tamas G, Soltesz I. Neurogliaform cells in the molecular layer of the dentate gyrus as feed-forward gamma-aminobutyric acidergic modulators of entorhinal-hippocampal interplay. J Comp Neurol. 2011; 519:1476–1491. [PubMed: 21452204]

Basu J, Zaremba JD, Cheung SK, Hitti FL, Zemelman BV, Losonczy A, Siegelbaum SA. Gating of hippocampal activity, plasticity, and memory by entorhinal cortex long-range inhibition. Science. 2016; 351:5694–5694.

Bezaire MJ, Soltesz I. Quantitative assessment of CA1 local circuits: Knowledge base for interneuron-pyramidal cell connectivity. Hippocampus. 2013; 23:751–785. [PubMed: 23674373]

Bragin A, Jandó G, Nádasdy Z, van Landeghem M, Buzsáki G. Dentate EEG spikes and associated interneuronal population bursts in the hippocampal hilar region of the rat. J Neurophysiol. 1995; 73:1691–1705. [PubMed: 7643175]

Ceranik K, Bender R, Geiger JR, Monyer H, Jonas P, Frotscher M, Lubke J. A novel type of GABAergic interneuron connecting the input and the output regions of the hippocampus. J Neurosci. 1997; 17:5380–5394. [PubMed: 9204922]

Girardeau G, Benchenane K, Wiener SI, Buzsáki G, Zugaro MB. Selective suppression of hippocampal ripples impairs spatial memory. Nat Neurosci. 2009; 12:1222–1223. [PubMed: 19749750]

Hájos N, Mody I. Synaptic communication among hippocampal interneurons: properties of spontaneous IPSCs in morphologically identified cells. J Neurosci. 1997; 17:8427–8442. [PubMed: 9334415]

Headley DB, Kanta V, Pare D. Intra- and inter-regional cortical interactions related to sharp wave ripples and dentate spikes. J Neurophysiol. 2016 jn.00644.2016.

Hosp JA, Struber M, Yanagawa Y, Obata K, Vida I, Jonas P, Bartos M. Morpho-physiological criteria divide dentate gyrus interneurons into classes. Hippocampus. 2014; 24:189–203. [PubMed: 24108530]

Hulse BK, Lubenov EV, Siapas AG, Hulse BK, Lubenov EV, Siapas AG. Brain State Dependence of Hippocampal Subthreshold Activity in Awake Mice Article Brain State Dependence of Hippocampal Subthreshold Activity in Awake Mice. CellReports. 2017; 18:136–147.

Katona L, Micklem B, Borhegyi Z, Swiejkowski DA, Valenti O, Viney TJ, Kotzadimitriou D, Klausberger T, Somogyi P. Behavior-dependent activity patterns of GABAergic long-range projecting neurons in the rat hippocampus. Hippocampus. 2016; 27:359–377.

Kron MM, Zhang H, Parent JM. The developmental stage of dentate granule cells dictates their contribution to seizure-induced plasticity. J Neurosci. 2010; 30:2051–2059. [PubMed: 20147533]

Lasztóczi B, Tukker JJ, Somogyi P, Klausberger T. Terminal Field and Firing Selectivity of Cholecystokinin- Expressing Interneurons in the Hippocampal CA3 Area. J Neurosci. 2011; 31:18073–18093. [PubMed: 22159120]

Lisman JE, Talamini LM, Raffone A. Recall of memory sequences by interaction of the dentate and CA3: A revised model of the phase precession. Neural Networks. 2005; 18:1191–1201. [PubMed: 16233972]

Melzer S, Michael M, Caputi A, Eliava M, Fuchs EC, Whittington MA, Monyer H. Long-Range–Projecting GABAergic Neurons Modulate Inhibition in Hippocampus and Entorhinal Cortex. Science (80-). 2012; 335:1506–1510.

Oliva A, Fernandez-Ruiz A, Buzsaki G, Berenyi A. Role of Hippocampal CA2 Region in Triggering Sharp-Wave Ripples. Neuron. 2016; 91:1342–1355. [PubMed: 27593179]

Penttonen M, Kamondi A, Sik A, Acsády L, Buzsáki G. Feed-forward and feed-back activation of the dentate gyrus in vivo during dentate spikes and sharp wave bursts. Hippocampus. 1997; 7:437–450. [PubMed: 9287083]

Sik, a, Ylinen, a, Penttonen, M., Buzsáki, G. Inhibitory CA1-CA3-hilar region feedback in the hippocampus. Science. 1994; 265:1722–1724. [PubMed: 8085161]

Szabadics J, Soltesz I. Functional specificity of mossy fiber innervation of GABAergic cells in the hippocampus. J Neurosci. 2009; 29:4239–4251. [PubMed: 19339618]

Szabó GG, Holderith N, Gulyás AI, Freund TF, Hájos N. Distinct synaptic properties of perisomatic inhibitory cell types and their different modulation by cholinergic receptor activation in the CA3 region of the mouse hippocampus. Eur J Neurosci. 2010; 31:2234–2246. [PubMed: 20529124]

Szabó GG, Papp OI, Máté Z, Szabó G, Hájos N. Anatomically heterogeneous populations of CB1 cannabinoid receptor-expressing interneurons in the CA3 region of the hippocampus show homogeneous input-output characteristics. Hippocampus. 2014; 24:1506–1523. [PubMed: 25044969]

Varga C, Golshani P, Soltesz I. Frequency-invariant temporal ordering of interneuronal discharges during hippocampal oscillations in awake mice. Proc Natl Acad Sci U S A. 2012; 109:E2726–34. [PubMed: 23010933]

Varga C, Oijala M, Lish J, Szabo GG, Bezaire M, Marchionni I, Golshani P, Soltesz I. Functional fission of parvalbumin interneuron classes during fast network events. Elife. 2014; 3:1–23.

Viney TJ, Lasztoczi B, Katona L, Crump MG, Tukker JJ, Klausberger T, Somogyi P. Network state-dependent inhibition of identified hippocampal CA3 axo-axonic cells in vivo. Nat Neurosci. 2013; 16:1802–1811. [PubMed: 24141313]

Wickersham IR, Sullivan HA, Seung HS. Production of glycoprotein-deleted rabies viruses for monosynaptic tracing and high-level gene expression in neurons. Nat Protoc. 2010; 5:595–606. [PubMed: 20203674]

## Highlights

1. GABAergic inputs to DG originate from extrinsic interneurons ($DG_{EXT}$)
2. Diversity of $DG_{EXT}$ cells is comparable to that of the intrinsic interneurons
3. $DG_{EXT}$ cells back-channel sharp wave-ripple (SWR) modulated inhibition to the DG
4. Extended interneuron system provides temporarily distributed inhibition to DG during SWRs

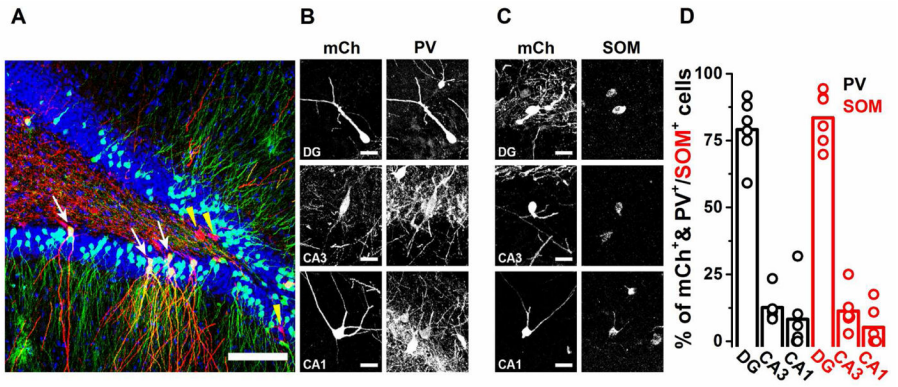


**Figure 1. Extrinsic interneurons located in CA3 and CA1 form a significant portion of GABAergic inputs to dentate granule cells (GCs)**

**(A)** Representative confocal image from the dentate gyrus (DG) of an animal that received injections of Syn-GTR at P7 and RbV-mCh at P126, and was euthanized 7 days later. $GFP^+/mCh^+$ cells (yellow) represent 'starter' DG GCs that were born at P7 (white arrows). Cells that are $mCh^+$ only (in red, denoted by yellow arrowheads) represent the first-order presynaptic inputs onto the starter GCs. Cell nuclei are visualized with bisbenzimide (blue). **(B–C)** Representative confocal images from the DG, CA3 and CA1 showing cells that are double positive for mCh and either PV or SOM. These cells provide monosynaptic inputs from DG, CA3 and CA1 onto neonatally-born DG GCs. **(D)** Quantification of the percentages of $PV^+$ or $SOM^+$ interneurons that arise from the DG, CA3 or CA1 and are monosynaptically connected to starter DG GCs (n=6 animals). Bars indicate means. Scale bars: 100μm (A) 25μm (B–C). For juxtacellularly labelled $DG_{INT}$ and $DG_{EXT}$ cell reconstructions see also Figs S1 and S2.

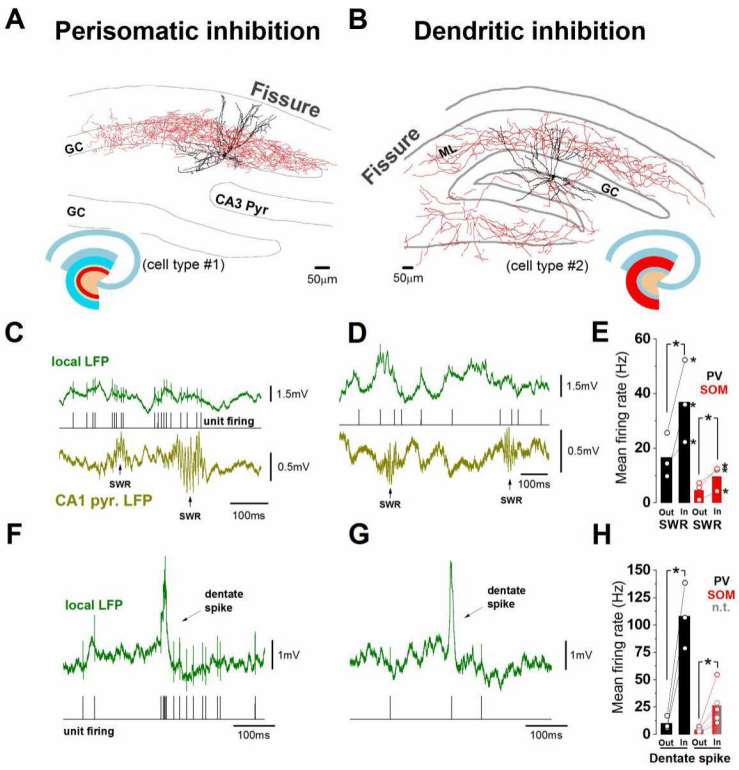


**Figure 2. Both perisomatic and dendritic inhibition in the dentate gyrus (DG) are modulated by sharp wave-ripples (SWRs)**

(**A–B**) Examples of perisomatic-targeting and dendrite-targeting cells. (**A**) Fast spiking basket cell (FSBC); (**B**) Total molecular layer innervating cell. Red: axon; black: soma and dendrite. Schematic drawings indicate the axonal coverage of the interneurons (red). (GC: granule cell layer; ML: molecular layer; Pyr: pyramidal layer). (**C–D**) Example traces showing SWR-modulated firing of cells in panels A and B. From top to bottom: local field potential, isolated action potentials, field potential recorded in CA1 pyramidal layer. (**E**) Significantly increased firing rate inside SWRs for PV perisomatic-targeting cells (in black, *P=0.041, t= −3.268, DF=2; n=3 for perisomatic-targeting cells) and at SOM dendrite-targeting cells (in red, *P=0.023, t=−4.547, DF=2, n=3 for SOM dendrite-targeting cells, paired t test; bars indicate means). All cells were significantly modulated individually as well (asterisks next to circles, $P<0.05$, see Methods). Note that out of five additional dendrite-targeting cells, one NOS cell had similarly increased firing during SWRs (#6 in Fig S1; outside SWR: 0.26Hz; inside SWR: 1.49Hz; see also Fig S3D, P<0.05, see methods), two neurochemically unidentified hilar neurons (n.t.; e.g. #3 in Fig S1E, see also Fig S3C) showed strongly reduced firing (outside SWR: 3.2Hz and 11.3Hz, inside SWR: 0Hz and 0Hz, respectively, P<0.05, see methods), two cannabinoid type I (CB1) receptor expressing cells (#5 in Fig S1B) were not significantly modulated (data not shown). (**F–H**) Example traces showing dentate spike-modulated firing of the same two cells shown on A and B. Top: local field potential; bottom: isolated action potentials. (**H**) Significantly increased firing rate of perisomatic- and dendrite-targeting cells inside dentate spikes (*$P$=0.01, t=−6.943, DF=2, $n$=3 and *$P$=0.016, t=−3.231, DF=4, $n$=5, respectively; paired t test; dendrite-targeting cells include two n.t. hilar neurons; mean of all dendrite-targeting cells indicated by red bars).

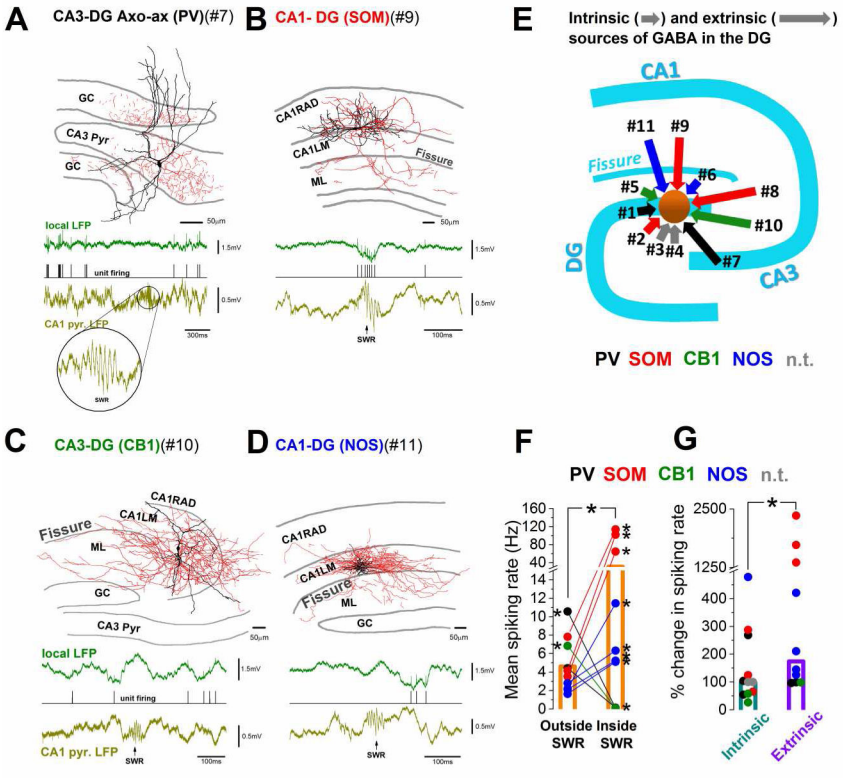


**Figure 3. Extrinsic GABAergic sources of the DG are modulated by sharp wave-ripples (SWRs)**

(**A**–**D**) Top: examples of extrinsically located cells expressing PV, SOM, CB1 or NOS (RAD: str. radiatum; LM: str. lacunosum-moleculare; ML: DG molecular layer; GS: granule cell layer; pyr: pyramidal layer). Red: axon; black: soma and dendrite. Bottom: example traces showing SWR-modulated firing of the corresponding cells. (**E**) Schematic summary of intrinsic and extrinsic sources of GABA in the DG. Color labels indicate neurochemical content and the lengths of arrows indicate the source (short arrow=$DG_{INT}$; long: $DG_{EXT}$). Cell numbers (#) are referring to cells shown in **A**–**D** and Figs S1and S2. Note that cell #8 projected to the hilus (see Fig S2E); n.t.: neurochemical identity not tested. (**F**) Significantly increased firing rate of extrinsic cells during (inside) *versus* outside SWRs ($P$=0.047, t=1.868, DF=9, $n$=10; paired t test). All cells were significantly modulated individually as well (asterisks next to filled circles, $P$<0.05, see Methods). **(G)** $DG_{EXT}$ cells show stronger SWR-related modulation than $DG_{INT}$ neurons (median[1st quartile, 3rd quartile]; $DG_{INT}$: 100[58.2, 268.6]; $DG_{EXT}$: 177.9[98.8, 1451.6]). P=0.04893, n=21, Z =−1.656, Mann-Whitney U test. Bars indicate medians.

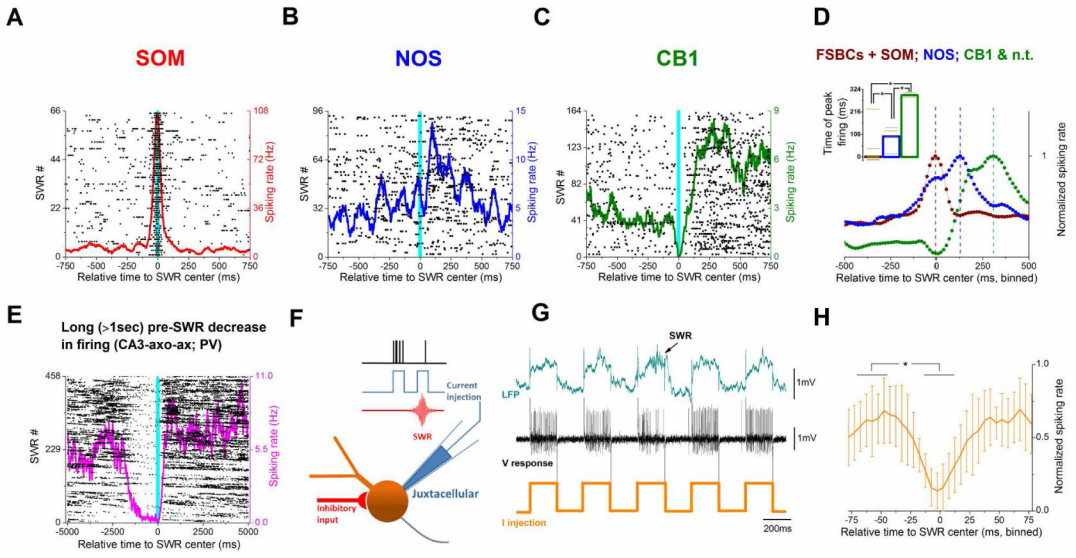


**Figure 4. Temporal dynamics of SWR-dependent modulation of interneuronal firing**

(**A–C**) Example raster plots (black dots) and spiking rate curves (in color) showing three typical patterns. Note the right-shifted positive peak with respect to SWR center (cyan bar) on **B** and **C**. (**D**) Three groups of interneurons whose discharges prefer distinct temporal windows relative to SWRs. Inset: summary of time of peak firing (vertical dashed lines on main panel) with respect to the middle of the SWRs (bars indicate median values): FSBCs +SOM (brown) 1.5[1$^{st}$ quartile: −8, 3$^{rd}$ quartile: 22.5]; NOS (blue): 98.5[56, 132]; CB1&n.t. (green) 296.5[285.5, 307.5] ($P$=0.0131, KW-ANOVA test, DF=2, n=16; completed with Mann-Whitney U test; *$P$=0.023, 0.017 and 0.041 (n=9, 2 and 5; Z=−2.00, −2.13 and 1.74) for brown vs. blue, brown vs. green and blue vs. green, respectively). (**E**) Example raster plot and spiking rate curve of an axo-axonic (chandelier) cell with a reduction in the firing rate that precedes SWRs by >1sec. Note the different time scale compared to **C**. (**F**) Experimental design for panels G and H. (**G**) Representative example of reduced firing rate when the strong current injection delivered through the juxtacellular pipette co-occurred with a SWR. (**H**) Significantly decreased spiking rate during SWRs in the experiments indicated in panels F and G. $n$=5, $P$=0.016, t=4.012, DF=4; paired t test.